

Sensing Paramagnetic Ions using T_1 relaxometry of NV-centres

Advait Risbud* Guide: Prof. Kasturi Saha †

May 6, 2024

Abstract

Since the discovery and characterisation of their fluorescence behaviour nearly 35 years ago, nitrogen-vacancy centres in diamond have become a hallmark in quantum sensing. The high stability and bio-compatibility of diamond NV-centres makes them incredibly versatile. One of the many applications of this system is in the detection of paramagnetic ions, whose magnetic noise distinctly alters the T_1 response of an NV-centre. By the careful characterisation and calibration of this response, it is possible to estimate the concentration of the paramagnetic ions in solution. In this project a series of FLIM and T_1 -relaxometry measurements have been done to study the interaction between NV-centers and ROS generated during the senescence process in mesenchymal stem cells.

*Department of Metallurgical Engineering and Materials Science, Indian Institute of Technology, Bombay
†Department of Electrical Engineering, Indian Institute of Technology, Bombay

Acknowledgement

I am incredibly thankful to Prof. Kasturi Saha for giving me the opportunity to work on this project. Every positive experience and lesson learned has shaped me into a better thinker and scientist. I also owe my thanks to Ayan Majumdar, Shishir Dashika, and Anuj Bathla for providing their unwavering support with the theory and experiments. Conversations and interactions with them have taught me more about being a scientist than other more established avenues have.

Contents

1	Introduction	5
1.1	Structure	5
1.2	Synthesis	6
1.3	Electronic Structure	6
2	Photoluminescence Kinetics in NV-centres	7
2.1	Relaxation Kinetics	7
2.2	Population Analysis	9
3	Nitrogen-Vacancy Centres in a Spin Bath	10
3.1	Effect of Magnetic Noise: Spherical Case	10
3.2	Effect of Magnetic Noise: Linear Case	11
4	Experimental Procedure	13
4.1	Experimental Setup	13
4.2	T_1 Protocol	15
4.3	Drift Calibration	15
5	Fluorescence Lifetime Imaging Microscopy (FLIM)	16
6	Results and Discussion	17
7	Future Directions	22

List of Figures

1	Unit Cell of a diamond lattice.	5
2	Structure of an NV-centre with C_{3v} symmetry.	5
3	HPHT synthesis of diamond. [1]	6
4	CVD growth of synthetic diamond with NV centres.[1]	7
5	Electronic Structure of the NV center. (c_1, c_2, c_3, n) are the molecular orbitals of the electrons.	8
6	Simplified 5-level diagram of the various relaxation pathways for the NV centre.	9
7	Single NV in a spin bath.[2]	10
8	Simulation of the rapid decrease in T_1 relaxation of a NV in a spherical nanodiamond as a function of the concentration of paramagnetic ions.	12
9	Layer of paramagnetic ions over a single NV.	12
10	Single-NV below a layer of paramagnetic ions, $L = 100\mu m$.	13
11	Simplified version of a confocal fluorescence microscope.	14
12	Confocal (left) v/s a wide-field (right) epifluorescence setup.	14
13	T_1 measurement protocol.	15
14	Combined schematic of T_1 and $g^2(\tau)$ measurement setup.	16
15	Drift measurements in confocal setup.	17
16	FLIM images of Hoechst dye and nanodiamonds inside the cells.	18
17	Histogram of nanodiamond fluoresense lifetimes.	19
18	T_1 measurement of nanodiamond at six different locations inside the cells.	20
19	Statistics of 300NV/ND samples outside of cells. Mean T_1 time is 182 μs .	21

1 Introduction

1.1 Structure

Carbon in its crystalline form, as diamond, is arranged in an FCC (face-centred cubic) arrangement. This arrangement is shown in the figure below (1). Each lattice point of the FCC is occupied by a tetrahedron of four carbon atoms with 4σ bonds connecting the corner atoms to the central carbon of the tetrahedron. This tetrahedron of carbon atoms along with the 4σ bonds constitutes the *basis* of the FCC lattice.

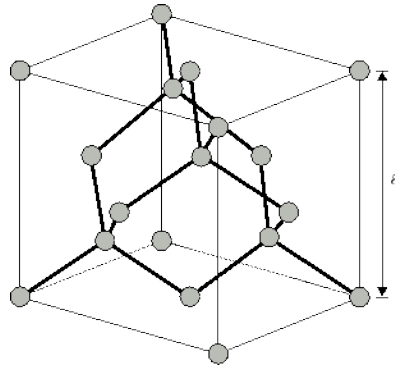


Figure 1: Unit Cell of a diamond lattice.

A perfect crystal of diamond would be transparent to visible light, owing to its extremely wide band gap of 5.48 eV ($\lambda \approx 226 \text{ nm}$ which is UV). However, on rare occasion naturally occurring diamond shows vivid colours due to the various defects inside it. Many defects have been studied inside diamond which lead to its fluorescence properties. These defects may be substitutional or vacancy or as in case of NV centres, both at the same time. These defects can be a consequence of the presence of impurities during the synthesis process or plastic deformation.

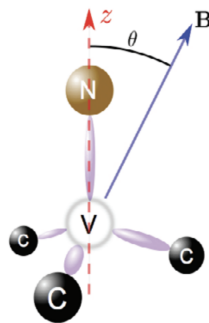


Figure 2: Structure of an NV-centre with C_{3v} symmetry.

If we replace two nearest neighbour carbon atoms with a nitrogen atom and a vacancy respectively, we get what is known as a nitrogen-vacancy centre defect. This defect comprises of a five-electron system which includes the three dangling bonds at the vacancy along with the lone-pair of electrons on the nitrogen. The defect traps an electron from the lattice and forms a charged NV-centre, denoted by NV^- .

1.2 Synthesis

The creation of the diamond with NV-centres starts by the synthesis of bulk diamond which is followed by further treatment to create the nitrogen impurity and the adjacent vacancy. Bulk diamond can be prepared by various techniques chief of which is HPHT (high-pressure, high-temperature) growth and chemical vapor deposition (CVD).

In HPHT synthesis a carbon source is put in contact with a seed diamond. The HPHT cell generates high pressure by keeping the seed inside a metal solvent, on which pressure is applied using anvils. The pressure is usually of the order of 5-7 GPa or higher. The cell is simultaneously heated to a high-temperature of 1,600-1,700 °c. Diamond produced by this procedure has nitrogen impurities dispersed within the crystal. Vacancies can be generated in these diamonds by irradiation with high-energy particles such as electrons, protons, and gamm particles. The substitutional nitrogen atom traps moving vacancies due to the increased lattice strain[1].

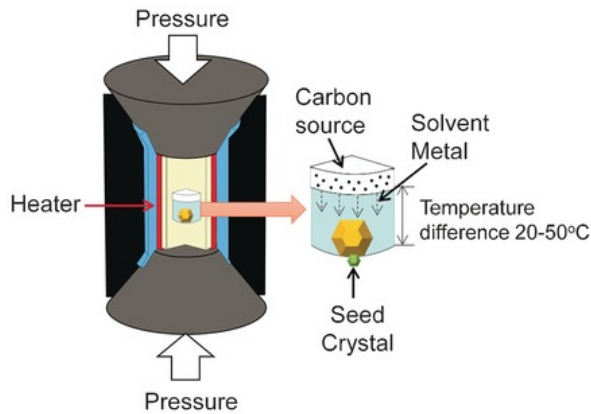


Figure 3: HPHT synthesis of diamond. [1]

An alternative way to grow synthetic diamond is chemical vapor deposition. A mixture of carbon-rich gases is used as the carbon source. This mixture is separated into individual atoms by a plasma arc. The carbon atoms assemble into a diamond film on a surface. Therefore CVD grown diamonds are obtained as thin films. Nitrogen-vacancy centres can be created inside these films by the growth of the film in presence of a gas mixture containing 0-0.1% N₂, 0.7% CH₄, and 99.2% H₂ [3].

1.3 Electronic Structure

The electronic structure of the NV⁻-centre has a C_{3v} symmetry. This space group consists of a three-fold axis of symmetry along the N-V direction and a σ_v plane of symmetry which contains the symmetry axis [4]. The distinguishing feature of a NV⁻ and NV⁰ centre are the zero-phonon lines at 1.945 eV (647 nm) and 2.156 eV (575 nm) respectively. The sharp ZPL absorption and well defined vibronic bands suggest that the NV-centre is a deep-level defect. The NV⁻ defect can also be identified by the zero field magnetic resonance at \approx 2.87 GHz. This corresponds to the 3A_2 triplet ground state. There is a second magentic resonance detected at \approx 1.42 GHz, this corresponds to the 3E triplet excited state. Applying the afformentioned microwave frequencies on an NV⁻ sample can drive oscillations between the $m_s = 0, \pm 1$ spin projections[5]. The NV-center defect exists as a deep-level defect inside the diamond band-gap. The NV⁻-center constitutes of 3 electrons from the

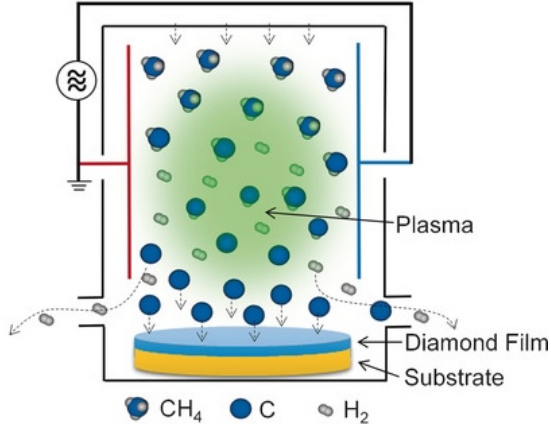


Figure 4: CVD growth of synthetic diamond with NV centres.[1]

dangling bonds of carbon atoms that surround the vacancy and the lone pair from the nitrogen atom. The defect also traps an electron from the lattice, making in total a six-electron system. The figure below shows the electronic structure generated by the linear combination of the sp^3 carbon atoms and the nitrogen lone-pair. The ground state Hamiltonian for the system can be written as follows

$$\mathcal{H}_{gs} = \hbar D_{gs} S_z^2 + g\mu_B \mathbf{B} \cdot \mathbf{S} \quad (1)$$

where D_{gs} is the ground-state zero-field splitting between the magnetic projections of $m_s = 0$, and $m_s = \pm 1$ and has value of 2.87 GHz. The NV-centre can be optically-excited to a spin triplet 3E state. The excited state zero-field splitting is given by $D_{es} = 1.42$ GHz. The NV-centre system can thus be modelled as an effective five-level model with one singlet state that can be reached via non-radiative relaxation (ISC). The figure (6) shows this model.

The system absorbs green light at 532 nm and emits a red line at 630 nm. Since the inter-system crossing is spin-dependent the system can be initialized to the $m_s = 0$ spin state and the spin-dependent PL allows for readout of the state. The next section outlines the kinetics of PL decay in NV centres.

2 Photoluminescence Kinetics in NV-centres

2.1 Relaxation Kinetics

The T_1 longitudinal relaxation time is defined as the time constant for decay of the system's fluorescence intensity. Measurement of this time constant gives us information about the rate of decay and changes in this rate can be attributed to a change in the local environment of the NV. This is what is observed in case of NVs that are placed in a spin bath. The magnetic noise from the spins causes a significant quenching in the relaxation time of the NV. We can quantify this quenching and relate it to the concentration of paramagnetic species around the NV-centre. To better understand the experimental procedure it is essential to elucidate the various relaxation pathways of the NV centre because it is these pathways that make T_1 relaxation measurement convenient for NV centres.

To study the fluorescence of the centre, the number of singlet states is not as important due to the spin-selective relaxation. Hence all single states have been merged into one, $|5\rangle$. It is evident from figure (6) that the spin-conserving transition are $|4\rangle \rightarrow |2\rangle$ and $|3\rangle \rightarrow |1\rangle$. The transition rates

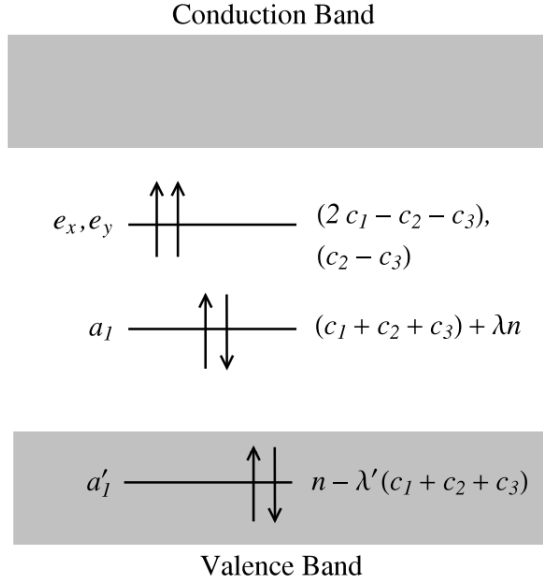


Figure 5: Electronic Structure of the NV center. (c_1, c_2, c_3, n) are the molecular orbitals of the electrons.

for these are given by k_{31} and k_{42} . Similarly the rates for the spin-flipping transitions are k_{41} and k_{32} . By optically exciting the centre, we would be populating the states $|3\rangle$ and $|4\rangle$. There are two main decay pathways that the system has, these are the radiative and non-radiative relaxations. So it is expected that the decay of the fluorescence intensity should be bi-exponential and the time constants would involve some combination of the decay rates out of state $|3\rangle$ and $|4\rangle$.

$$T_{1,|3\rangle} = 1/(k_{31} + k_{32} + k_{35}) \quad (2)$$

$$T_{1,|4\rangle} = 1/(k_{41} + k_{42} + k_{45}) \quad (3)$$

The expression for the bi-exponential fluorescence intensity decay can be written as,

$$\mathcal{I}(\tau) = \mathcal{I}(\infty)[1 - C_m e^{-\tau/T_m} + C_1 e^{-\tau/T_1}], \quad (4)$$

where T_m and T_1 are time-constants for the non-radiative and radiative relaxation pathways respectively.¹ The non-radiative relaxation happens on a much faster timescale (ns) than what we are concerned with in T_1 measurements (μs).

$$T_{1,|5\rangle} = T_m = 1/(k_{52} + k_{51}) \quad (5)$$

So for the most part we can ignore the faster relaxation schemes and focus on the slower, radiative relaxation which is useful for sensing applications.

$$\mathcal{I}(\tau) = \mathcal{I}(\infty)[1 + C_1 e^{-\tau/T_1}] \quad (6)$$

In (4) C_m is the PL contrast coefficient for the metastable quenching processes (i.e the non-radiative relaxation due to inter-system crossing) and C_1 is the PL contrast coefficient for the radiative quenching process [2]. To calculate the value of the C_1 contrast coefficient we can undertake an analysis

¹The subscript "m" denotes that the non-radiative relaxation is from a metastable singlet state.

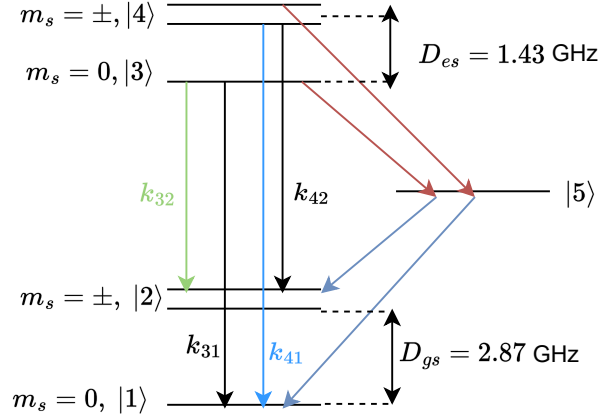


Figure 6: Simplified 5-level diagram of the various relaxation pathways for the NV centre.

of the probability of the NV occupying a particular spin state. This also leads to the bi-exponential decay expression as stated in (4).

In summary, it is observed that the decay out of $|3\rangle$ into $|5\rangle$ is much slower than from $|4\rangle$ into $|5\rangle$. However, the rate of decay out of $|5\rangle$ into $|2\rangle$ and $|1\rangle$ is equal [2]. Hence upon optical excitation into the 3E excited state, the system finally relaxes with a greater probability into the $|1\rangle$ state. This shows that the spin-selective relaxation leads to a polarisation of the spin-state of the system. This polarisation can be used to initialise the spin of the NV-centre into the $m_s = 0$ spin projection following which optical read-out of the spin state is also possible. The optical read-out is done by comparing the fluorescence intensity of the system with that of a system which is prepared in the $m_s = 0$ or $m_s = \pm 1$ state.

2.2 Population Analysis

The state of the NV-centre can be initialized by optically pumping with a 532 nm laser. This excites the system from the thermal equilibrium state wherein each spin-state ($m_s = 0, \pm 1$) is equally populated, to one where the probability of occupation is polarized to the $m_s = 0$ state. The probability of occupying the $m_s = 0, \pm 1$ states is given by

$$p_0(\tau) = \frac{1}{3} + \left[p_0(0) - \frac{1}{3} \right] e^{-\tau/T_1} \quad (7)$$

$$p_{\pm 1}(\tau) = \frac{1}{3} \pm \left[\frac{p_{+1}(0) - p_{-1}(0)}{2} \right] e^{-\tau/(3T_1)} - \frac{1}{2} \left[p_0(0) - \frac{1}{3} \right] e^{-\tau/T_1} \quad (8)$$

The PL readout $\mathcal{I}(\tau)$ can be written as

$$\mathcal{I}(\tau) = A_0 n_0(\tau) + A_1 [n_{+1}(\tau) + n_{-1}(\tau)] \quad (9)$$

where A_0 and A_1 are rates associated with the emission from the $m_s = 0$ and $m_s = \pm 1$ states respectively [6]. As discussed previously, the emission rate from the $m_s = 0$ state is much higher than from the $m_s = \pm 1$ state hence we can say that $A_0 > A_1$ and reduce the expression for PL intensity to (6). Fluorescence decays are usually modelled through exponential functions, however this

need not always be true such as in the case of delayed fluorescence (DF). The contrast coefficient C is given by

$$C = (3n_0(0) - 1) \frac{A_0 - A_1}{A_0 + 2A_1}. \quad (10)$$

Hence it depends on the degree of initial polarization and the difference in fluorescence intensity of the two pathways.

3 Nitrogen-Vacancy Centres in a Spin Bath

The chief utility of the NV centre is in that its fluorescence changes based on the environment. In this section the effect of magnetic noise on the fluorescence properties of the NV centre has been elucidated. A paramagnetic ion has a magnetic dipole moment which interacts with the dipole moment of the NV-centre. The paramagnetic ion creates a varying magnetic field at the location of the central spin, $\langle B(t) \rangle$. This magnetic noise causes a change in the T_1 relaxation time of the central spin. The change in relaxation is extremely sensitive to the concentration of paramagnetic ions and hence can be used for sensing the same.

3.1 Effect of Magnetic Noise: Spherical Case

Consider a single NV-centre that is trapped at the core of a nanodiamond. Let there be a σ surface density of paramagnetic ions on the surface of the nanodiamond, and a σ_s density of surface charges. The surface charges as well as the paramagnetic ions contribute to the change in T_1 relaxation time of the central spin. The setup has been given in figure (7).

Here the r_i is the distance of the the i^{th} spin from the central spin and \vec{u}_i is the unit vector along

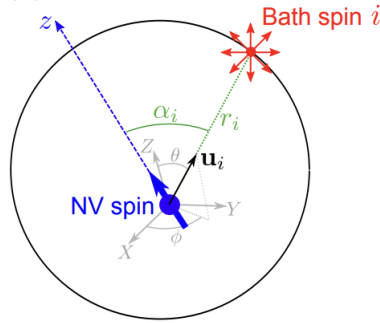


Figure 7: Single NV in a spin bath.[2]

the line joining the central spin and NV-centre. Note that the quantization axis of the central spin is assumed to be along the z-axis. The magnetic field at the central spin due to the paramagnetic/surface spin (note that the noise from paramagnetic spins and surface spins is characterised in the same manner and differ only by a multiplicative factor)

$$\vec{B}_i = \frac{\mu_0 \gamma_e \hbar}{4\pi r_i^3} [\vec{S}_i - 3(\vec{S}_i \cdot \vec{u}_i)\vec{u}_i] \quad (11)$$

Since only the transverse component of the magnetic field will affect the central spin,

$$\begin{aligned} B_{\perp}^2 &= \sum_i B_{\perp,i}^2 \\ &= \sum_i \langle B_{x,i} \rangle^2 + \langle B_{y,i} \rangle^2 \\ &= \sum_i \text{Tr}\{\rho(B_{x,i}^2 + B_{y,i}^2)\} \\ &= \sum_i \left(\frac{\mu_0 \gamma_e \hbar}{4\pi}\right)^2 C_S \frac{2 + 3 \sin^2 \alpha_i}{r_i^6} \end{aligned}$$

The expectation is taken over the thermally mixed state for both interacting spins, the density matrix for which is

$$\rho = \frac{1}{2S+1} \mathbb{1}_{2S+1} \otimes \mathbb{1}_{2S+1}$$

and from this we get,

$$C_S = \frac{1}{2S+1} \sum_{m=-S}^{m=S} m^2 = \frac{S(S+1)}{3}$$

Integrating the expression for the magnetic field over the surface of the nanodiamond we obtain the following expressions for the magnetic field due to the surface charge, and paramagnetic ions (Gd^{+3} in this case).

$$B_{\perp,surf}^2 = \left(\frac{\mu_0 \gamma_e \hbar}{\pi}\right)^2 C_{s,surf} \pi \frac{\sigma_{surf}}{(d_0/2)^4} \quad (12)$$

$$B_{\perp,Gd}^2 = \left(\frac{\mu_0 \gamma_{Gd} \hbar}{\pi}\right)^2 C_{s,Gd} \pi \frac{\sigma_{Gd}}{(d_0/2 + l)^4} \quad (13)$$

Here d_0 and l are the diameter of the nanodiamond (since NV spin is assumed to be at the geometric centre this is also the distance to the surface spins) and distance of the layer of paramagnetic ions from the surface of the nanodiamond respectively. The values for σ_{surf} have to be calculated iteratively with input from experiment. The authors of [2] approximate the density of surface spins to be $\approx 1 \text{ nm}^{-2}$. The value of T_1 can be calculated using the expression below.

$$\boxed{\frac{1}{T_1} = \frac{1}{T_{1,bulk}} + 3\gamma_e^2 B_{\perp,Gd}^2 \frac{R_{dip}}{R_{dip}^2 + \omega_0^2} + 3\gamma_e^2 B_{\perp,s}^2 \frac{R_s}{R_s^2 + \omega_0^2}} \quad (14)$$

Here R_s and R_{dip} are the fluctuation rates of surface and paramagnetic spins respectively. These fluctuation rates are the inverse of the correlation time (τ_c) for the magnetic noise produced by the surface and paramagnetic spins.

3.2 Effect of Magnetic Noise: Linear Case

Consider now the case shown in the figure below. There is a layer of paramagnetic ions above a single NV-spin. The layer of ions is at a distance t from the single NV. Calculation of the T_1 for this case can be done by modifying the expression for the magnetic field by performing a coordinate transform. Let the origin of the coordinates be at the position of the central spin. Consider a paramagnetic ion

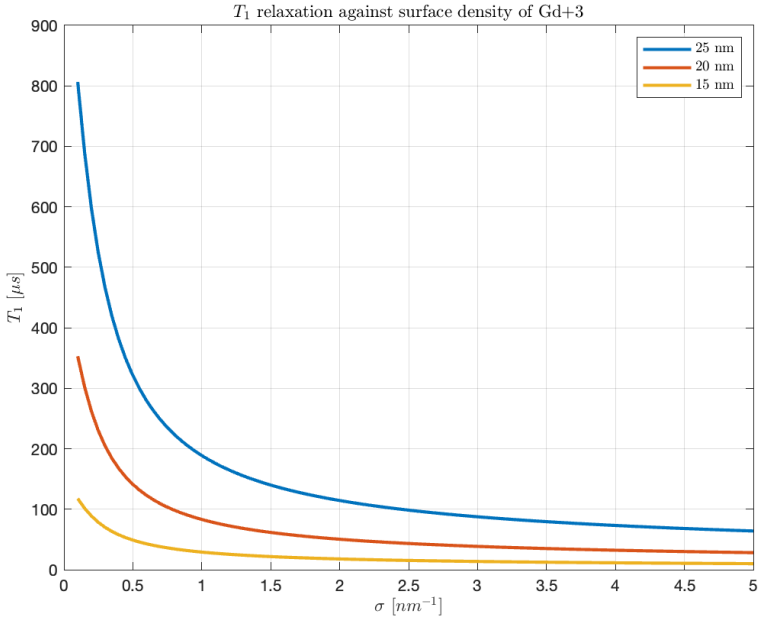


Figure 8: Simulation of the rapid decrease in T_1 relaxation of a NV in a spherical nanodiamond as a function of the concentration of paramagnetic ions.

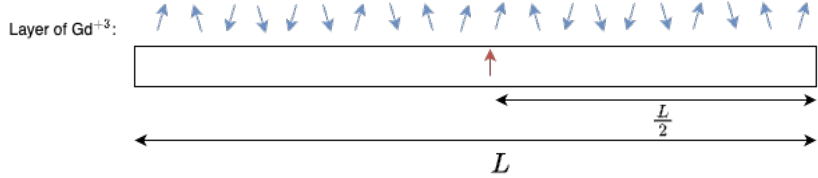


Figure 9: Layer of paramagnetic ions over a single NV.

at a distance (x, t) ,

$$\begin{aligned} r &= \sqrt{x^2 + t^2} \\ \theta &= \arcsin \frac{x}{r} \\ f &= \left(\frac{\mu_0 \gamma_e \hbar}{4\pi} \right)^2 C_S \left(\frac{2 + 3 \sin^2 \theta}{r^6} \right) \end{aligned}$$

The function f is integrated over x from $[-\frac{L}{2}, \frac{L}{2}]$ to get B_\perp^2 . The change in T_1 relaxation as a function of linear density of NVs is shown below, for different distances between the single-NV and the layer of paramagnetic ions (once again considered to be Gd^{+3}). Once again we see that with an increase in the linear density of paramagnetic ions the relaxation time decreases drastically. This is a Gedankenexperiment, but will help in modelling a layer of NVs below a layer of paramagnetic ions. In further work, this model will be extended to a 2-D system with a fixed density of NV-centres below a varying surface density of paramagnetic ions. The model can help to characterise such chips

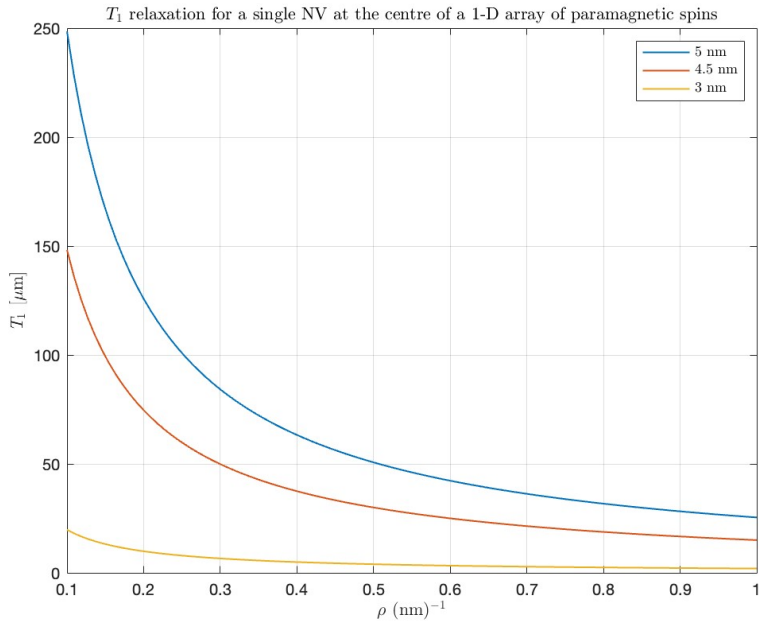


Figure 10: Single-NV below a layer of paramagnetic ions, $L = 100\mu\text{m}$.

developed for sensors by identifying the distribution of T_1 relaxation time given a certain density of NVs. This would constitute further work done as a part of the project.

4 Experimental Procedure

Fluorescence measurements are one of the most important tools in a physical chemist's toolbelt and there is a large array of techniques that are used to probe different fluorescence related phenomena in an equally large array of materials. In the case of NV-centres since we are interested in probing the fluorescence of features that are in the order of a few nm, it is imperative to use techniques with a higher resolution than ensemble measurements. Borrowing from the well-established area of single-molecule spectroscopy, we perform confocal microscopy on a sample of NV centres. The basic components of a fluorescence microscope are: a light source, dichroic mirrors, excitation and emission filters, objective lens, sample stage, detectors. Each of these components play a crucial in acquiring reliable fluorescence data.

4.1 Experimental Setup

Since our system absorbs green light at 530 nm, a 532 nm green laser is used for the excitation. The 532 nm light comes from the second-harmonic generation of 1064 nm He-Ne laser. The red-light which is emitted by the NVs is collected in an epifluorescence setup. This means that the emitted light travels in the reverse direction of the excitation light is separated from the excitation light using a dichroic filter. The emission is collected on a CCD (charge-coupled device) camera, as shown in the figure below.

The resolution of the measurement can be increased by using a confocal excitation instead of a

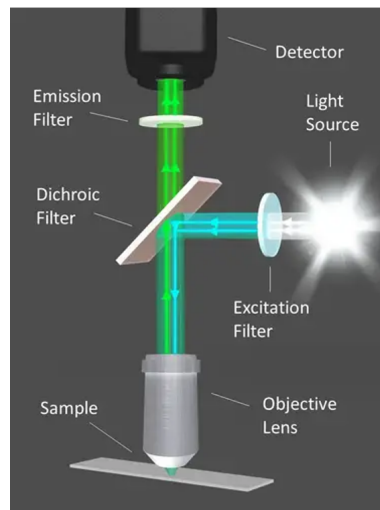


Figure 11: Simplified version of a confocal fluorescence microscope.

wide-field arrangement. The confocal region creates a very narrow excitation zone in the sample, and from the size of the excitation one can ascertain the number of molecules that are being excited at a time. The figure below shows the difference between a confocal and a wide-field setup. The key difference in the arrangements lies in the use of different lenses in the light path. There are

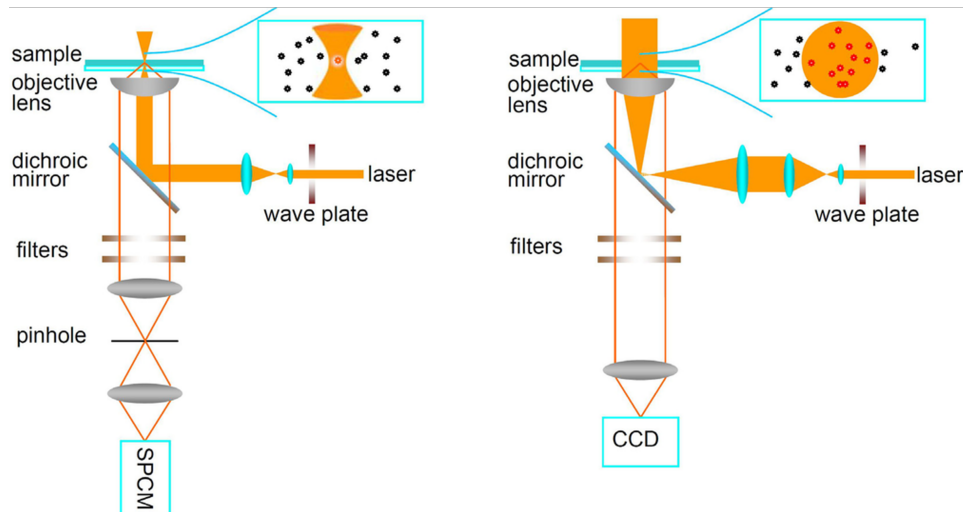


Figure 12: Confocal (left) v/s a wide-field (right) epifluorescence setup.

advantages to both setups however a confocal setup gives the user spatial selectivity in excitation. Therefore different regions of the sample are excited one after the other. The process of scanning one region of the sample after another in grid-like fashion is called "raster scanning". To allow for this motion a movable piezoelectric stage of dimensions $200\mu m \times 200\mu m \times 200\mu m$ is used. For the epifluorescence setup to work as desired the dichroic mirror is an essential component. The dichroic mirror allows light above a certain wavelength to pass and reflects the remaining light. So for imaging

NVs the range of dichroic should be such that it reflects the green light and transmits the red light which is then collected at the camera. The measurements in cell samples are done by focusing the sample under white light. This allows us to locate the layer in which cells are present.

4.2 T_1 Protocol

The T_1 pulse protocol for the NV-center is analogous to the spin-lattice relaxometry done in the case of NMR measurements. First the spin-state of the NV center is polarised to the $m_s = 0$ state. The spin-selective relaxation property of the NV-center comes into play here. The time period of this pulse must be optimised based on the number density of NV centers in a particular nanodiamond. For instance, the nanodiamonds used in this study with 300 NV/ND require a polarisation time of 100 μs to be sufficiently polarised into the $m_s = 0$ state. The fluorescence of the system is recorded for a duration of 1200 ns, this readout pulse is given to the DAQ with a delay pulse. The system is then left to relax for a dark time ' τ '. This dark time is varied in order to observe the decay in population of the $m_s = 0$ state. The laser source gives a continuous wave output and so to create a



Figure 13: T_1 measurement protocol.

pulse as shown below, an acousto-optic modulator must be used. An acousto-optic modulator uses the change in refractive index of a material by applying an acoustic wave. This leads to diffraction of the incident continuous wave laser. The apparatus is designed such that the first-order maxima gets the highest intensity. To create a pulse, the AOM is given a pulse power, such that when it is off only the zeroth order maxima appears. However the lenses are aligned such that only the first order maxima is collected, hence when the AOM is off there is no first order maxima thus no light passes [7].

4.3 Drift Calibration

Every confocal microscope has a nanopositioning system as one of its most essential components. This allows the user to look at different parts of the sample with nanometer precision. The nanopositioning system used in the PQuest lab is the NanoDrive LPS200. The system has 3-degrees of freedom and $200 \mu\text{m} \times 200 \mu\text{m} \times 200 \mu\text{m}$ range of motion. Such accurate motion is achieved via a piezoelectric stage that uses the expansion and contraction of a piezoelectric crystal upon application of a voltage to move the sample. Due to variations in temperature there is thermal drift in the position of the stage. If left uncorrected, it can lead to errors in measurement such as noisy T_1 data and grainy confocal images.

The drift in an extremely sparse nanodiamond sample was recorded overnight for a duration of 13.5 hours. The data comprises of 18 scans of the nanodiamond region divided into 300×300 pixels. The integration time at each pixel was 15 μs with 10 averages. Each scan lasted for 900 seconds. The figure below shows the trajectory of the most intense point on the nanodiamond overnight. The brightest point in the images was localized using a clustering algorithm. A brute force MAX(image) method does not work as there can be noisy pixels with high intensities, this can lead to erroneous localization.

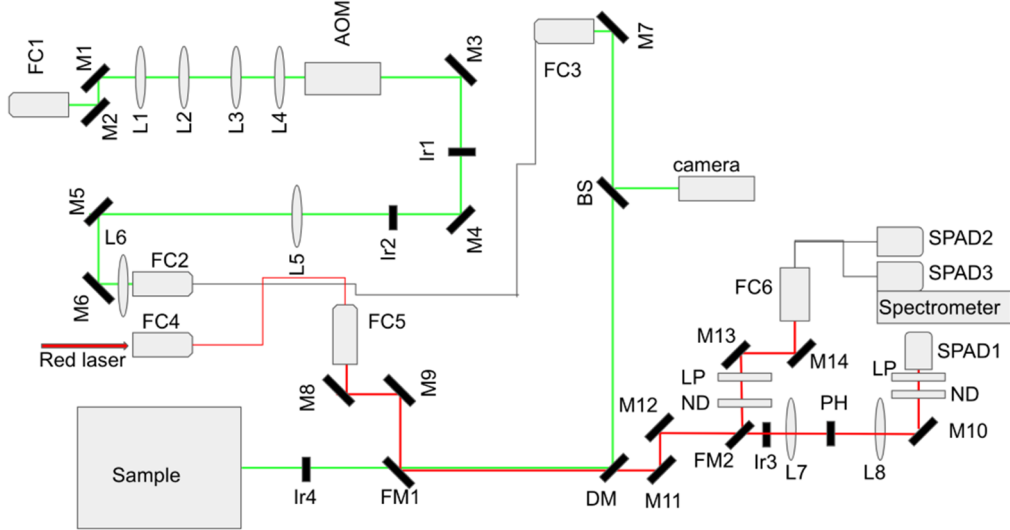


Figure 14: Combined schematic of T_1 and $g^2(\tau)$ measurement setup.

The key inference from this experiment was that the thermal drift was of the order of 1-2 μm over a 12+ hour period. The time needed for the T_1 sequence to run is approximately 32 minutes. So over the time scale of our concern we need not worry about defocusing due to drift given that we are looking at diffraction limited spots.

5 Fluorescence Lifetime Imaging Microscopy (FLIM)

FLIM is a technique used to perform simultaneously spectroscopy and microscopy of samples. This is a confocal microscopy technique where the sample is placed on a nanopositioning system in an epifluorescence measurement setup. As each point on the sample is scanned, a time-correlated single photon counting (TCSPC) measurement is done at each pixel. The sample is optically excited and the lifetime is measured using a pulse sequence. This is an ultrafast measurement technique, and with the added advantage of microscopy one can probe the heterogeneity in lifetime over different regions of the sample. From the variation in lifetime it is possible to make inferences about the local environment for example the presence of quenchers, or excited state processes. A TCSPC measurements involves a "START" pulse which excites the sample and a "STOP" pulse. When an emitted photon hits the detector the "STOP" pulse is generated. The time between the two pulses is varied to look at the variation of photon arrival frequency with time. This is used to build up a histogram, and using a convolution with the instrument response function the decay kinetics of the optically excited state are determined. When this process is repeated at many points inside a sample, we can generate a lifetime-weighted fluorescence image of the sample.

Inside the cells there are two fluorophores, the Hoechst dye which is used to stain the nucleus, and the nanodiamonds. To image each fluorophore the optical filters and dichroic mirrors need to be changed. Below are the emission and absorption spectrum for Hoechst dye and NV centers in diamond. The dye is excited at 404 nm and the emission is recorded at 532 nm. A 404/532 nm dichroic mirror is placed in the detection path for the Hoechst dye with a 425 nm low-pass filter.

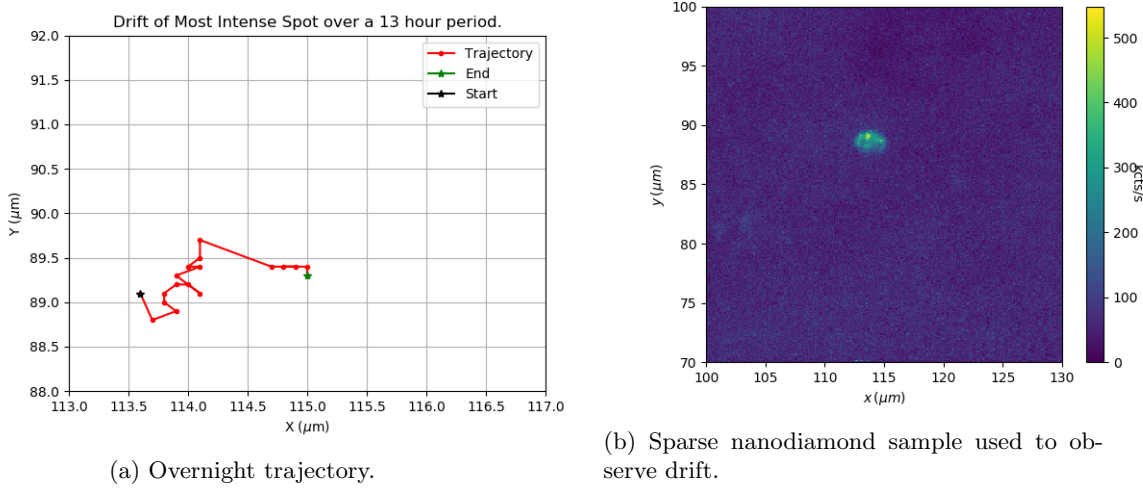


Figure 15: Drift measurements in confocal setup.

The cells that have been incubated with the nanodiamonds and Hoechst dye are placed between two glass coverslips, and this sandwich is placed on the stage of the confocal microscope. For obtaining focused imaged, we first look for a region of the sample where there are cells in only a single layer. This means that even if there is z-drift in the stage no new cells would get focused and only the existing cells would get defocused. This is also not ideal, however it is easier to identify than if a new cell comes into focus. Once the sample has been focused, a snapshot of the widefield microscope image is taken and thereafter FLIM is done for the Hoechst dye as well as the NV centers.

Observing a change in the lifetime of the dye is not the focus of this study, hence the FLIM image of the dye is helpful for identifying where the dye has deposited in the cell and comparing it with the position of the NV centers.

6 Results and Discussion

Stem cells that have been incubated for 24 hours without ROS and subsequently fixed have been imaged using FLIM. We can see that the Hoechst dye adheres to the nuclei of the cells, while the nanodiamonds are dispersed within the cytoplasm. Some of the nanodiamonds are present as larger clusters while others are more disperse. A pertinent question to ask here is why such a distribution of nanodiamonds is seen inside the cell, which will be the subject of further study. Along with this we see some heterogeneity in the lifetimes of the nanodiamonds however the variance is quite low as can be inferred from the histograms of the lifetimes for nanodiamonds 17.

Further, T1 measurements were performed at six different regions in the sample 18. Since there are no ROS added to the cells we should expect the T1 relaxation time to be similar to that of the same nanodiamonds outside of the cell. Statistics on T1 values of nanodiamonds on the 300NV/ND sample and the histogram has been shown below. As expected the measurements in the cells ($\mu = 176 \text{ ns}$) matches closely to the T1 value for the nanodiamonds outside of the cell.

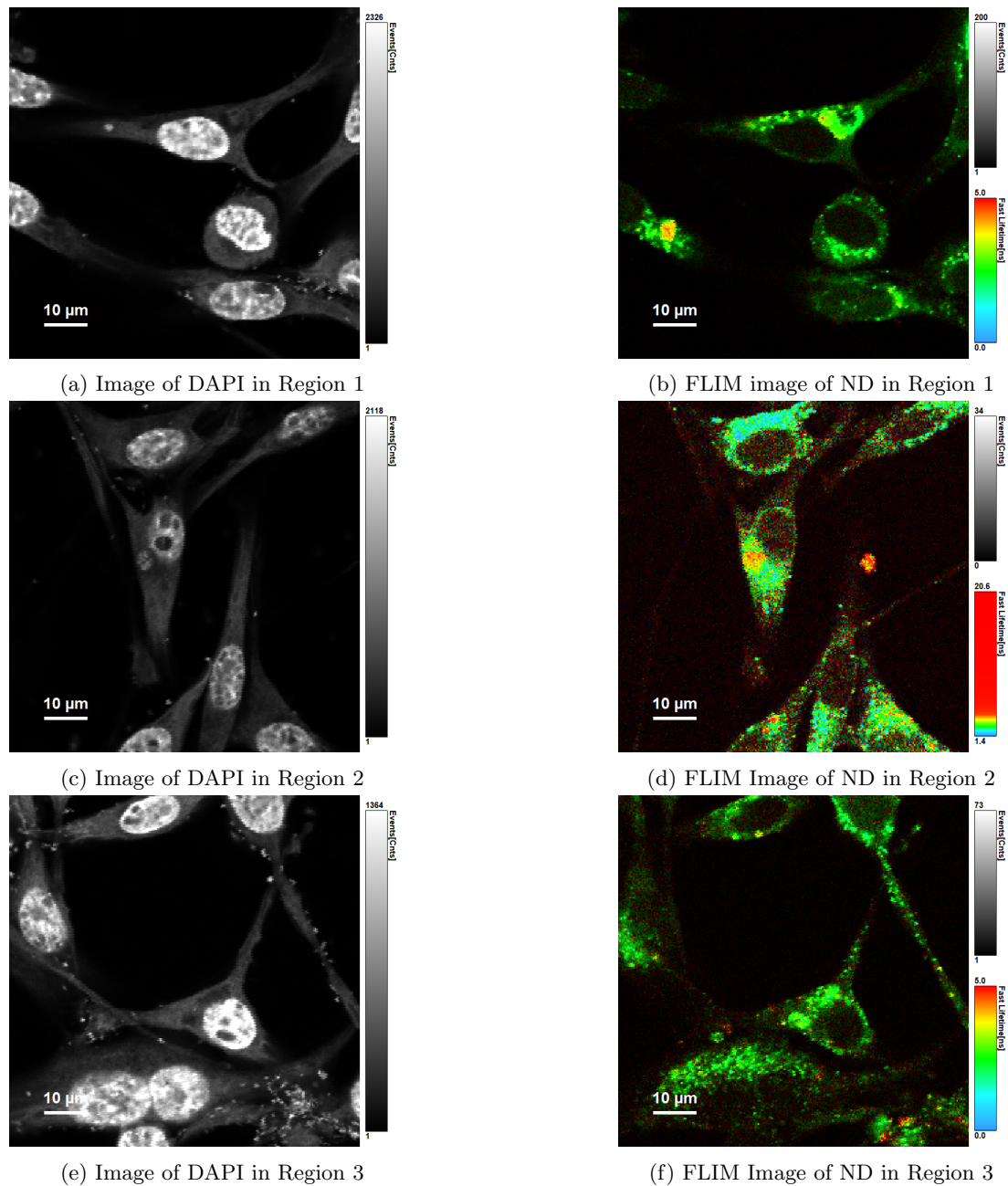
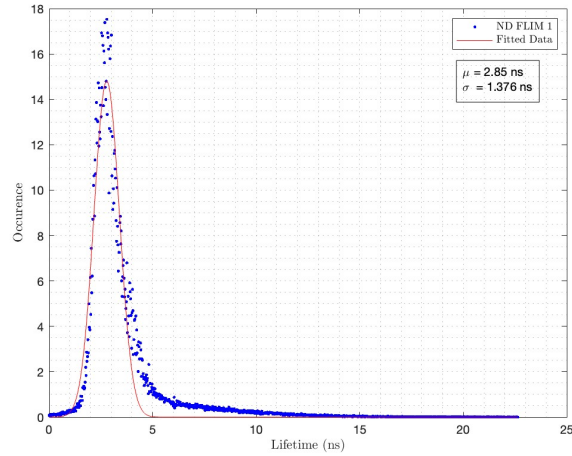
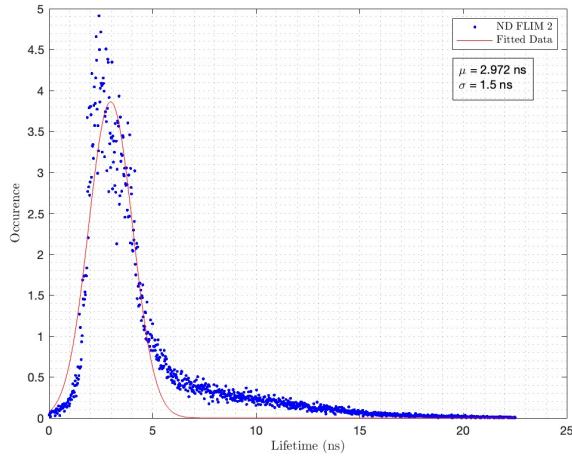


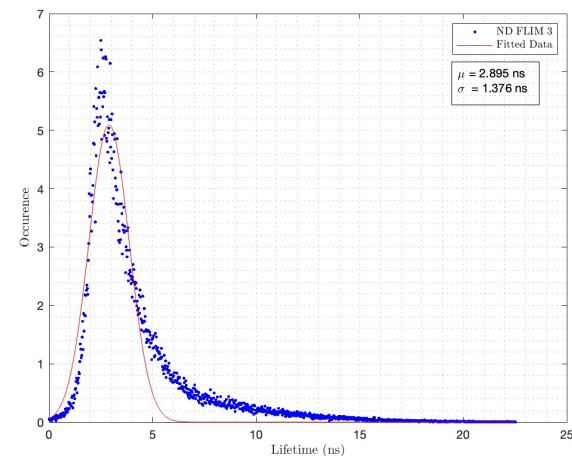
Figure 16: FLIM images of Hoechst dye and nanodiamonds inside the cells.



(a) Distribution of lifetimes for nanodiamonds in region 1.
Mean lifetime is 2.85 ns and variance is 1.376 ns.



(b) Distribution of lifetimes for nanodiamonds in region 2.
Mean lifetime is 2.972 ns and variance is 1.5 ns



(c) Distribution of lifetimes for nanodiamonds in region 3.
Mean lifetime is 2.895 ns and variance is 1.375 ns.

Figure 17: Histogram of nanodiamond fluorescence lifetimes.

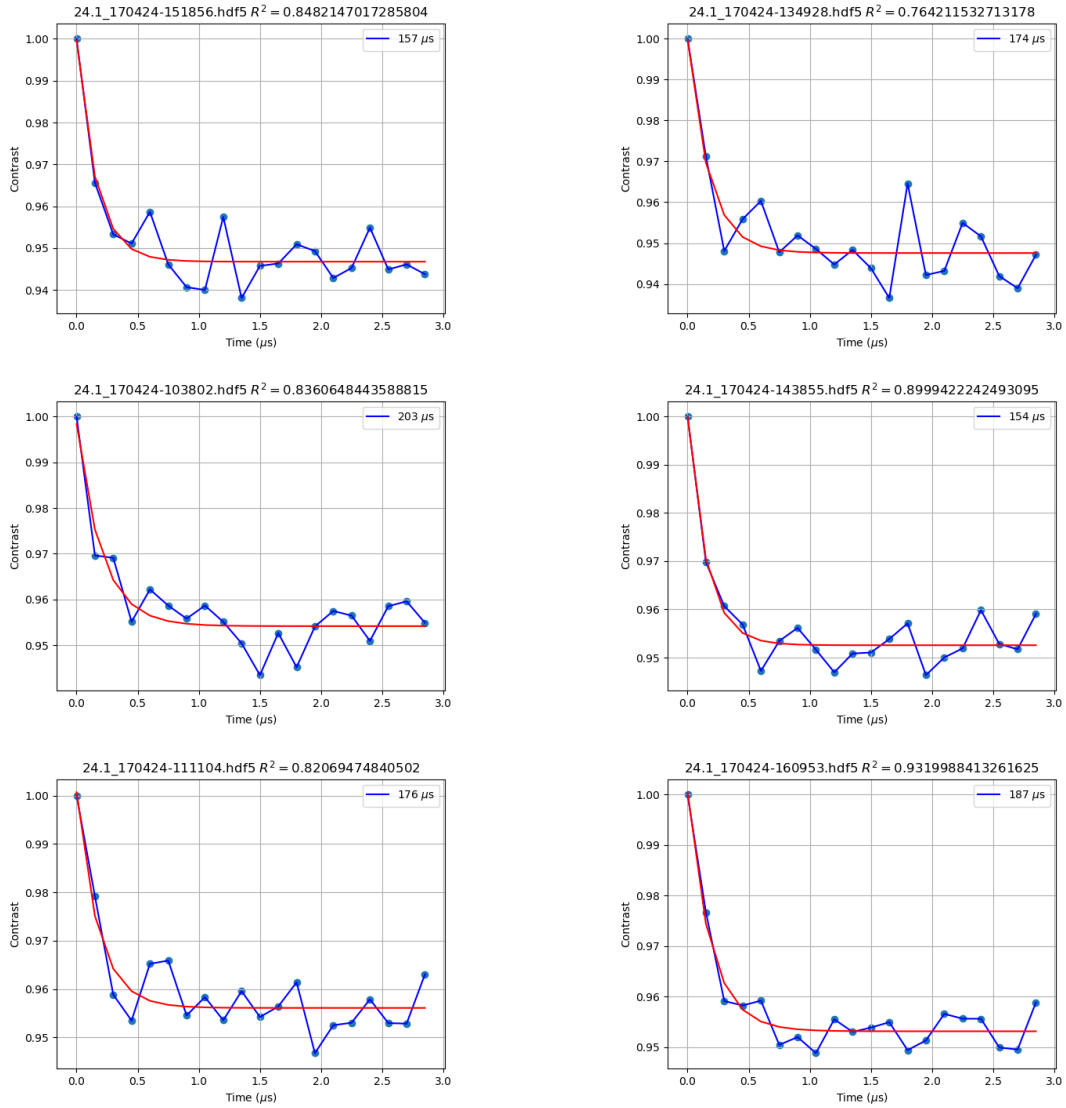


Figure 18: T1 measurement of nanodiamond at six different locations inside the cells.

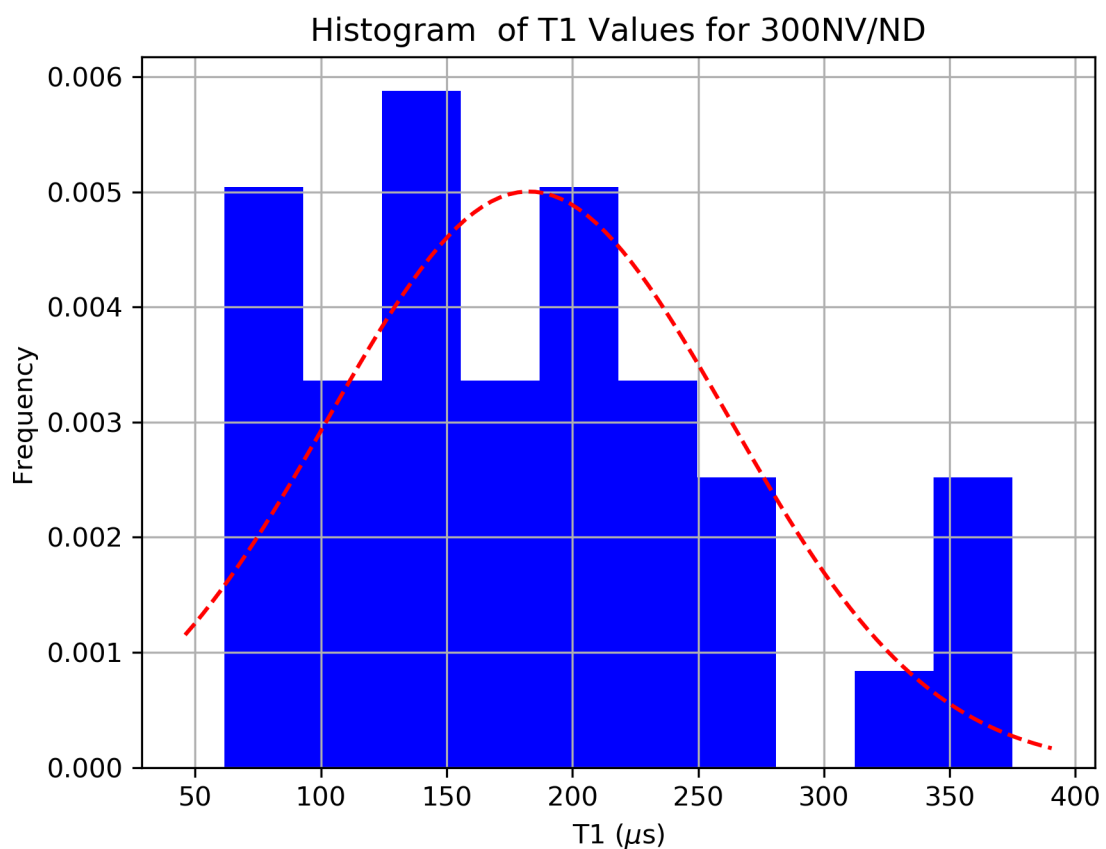


Figure 19: Statistics of 300NV/ND samples outside of cells. Mean T1 time is 182 μ s.

7 Future Directions

Further work on this project will involve proof of change in T_1 relaxation times as a consequence of different concentrations of ROS. It will also be interesting to look at any heterogeneities in lifetime as well as longitudinal relaxation time between clusters of different sizes of nanodiamonds. The reasons behind differential clustering of nanodiamonds inside cells are not clear. Looking into the distribution of nanodiamonds inside the cells could provide useful insight into the transport pathways of micrometers sized particles inside cells, and will inform future experiments in tagging of cell organelles using antibodies for targetted imaging and sensing. T_1 relaxometry using NV centers has been used for sensing other radical-mediated life processes such as hypoxia and regeneration [8].

References

- [1] Yuzhou Wu, Fedor Jelezko, Martin B Plenio, and Tanja Weil. Diamond quantum devices in biology. *Angewandte Chemie International Edition*, 55(23):6586–6598, 2016.
- [2] J.-P. Tetienne, T. Hingant, L. Rondin, A. Cavaillès, L. Mayer, G. Dantelle, T. Gacoin, J. Wrachtrup, J.-F. Roch, and V. Jacques. Spin relaxometry of single nitrogen-vacancy defects in diamond nanocrystals for magnetic noise sensing. *Phys. Rev. B*, 87:235436, Jun 2013.
- [3] J. R. Rabeau, S. T. Huntington, A. D. Greentree, and S. Prawer. Diamond chemical-vapor deposition on optical fibers for fluorescence waveguiding. *Applied Physics Letters*, 86(13):134104, 03 2005.
- [4] J-P Tetienne, L Rondin, P Spinicelli, M Chipaux, T Debuisschert, J-F Roch, and V Jacques. Magnetic-field-dependent photodynamics of single nv defects in diamond: an application to qualitative all-optical magnetic imaging. *New Journal of Physics*, 14(10):103033, oct 2012.
- [5] Marcus W. Doherty, Neil B. Manson, Paul Delaney, Fedor Jelezko, Jörg Wrachtrup, and Lloyd C.L. Hollenberg. The nitrogen-vacancy colour centre in diamond. *Physics Reports*, 528(1):1–45, 2013. The nitrogen-vacancy colour centre in diamond.
- [6] Changhao Li, Mo Chen, Dominika Lyzwa, and Paola Cappellaro. All-optical quantum sensing of rotational brownian motion of magnetic molecules. *Nano Letters*, 19(10):7342–7348, 2019. PMID: 31549847.
- [7] Dominik B. Bucher, Diana P. L. Aude Craik, Mikael P. Backlund, Matthew J. Turner, Oren Ben Dor, David R. Glenn, and Ronald L. Walsworth. Quantum diamond spectrometer for nanoscale nmr and esr spectroscopy. *Nature Protocols*, 14(9):2707–2747, Sep 2019.
- [8] Siyu Fan, Han Gao, Yue Zhang, Linyan Nie, Raquel Bártolo, Reinier Bron, Hélder A. Santos, and Romana Schirhagl. Quantum sensing of free radical generation in mitochondria of single heart muscle cells during hypoxia and reoxygenation. *ACS Nano*, 18(4):2982–2991, 01 2024.